

pubs.acs.org/NanoLett Letter

Symmetry-Broken Chern Insulators in Twisted Double Bilayer Graphene

Minhao He, Jiaqi Cai, Ya-Hui Zhang, Yang Liu, Yuhao Li, Takashi Taniguchi, Kenji Watanabe, David H. Cobden, Matthew Yankowitz,* and Xiaodong Xu*



Cite This: Nano Lett. 2023, 23, 11066-11072



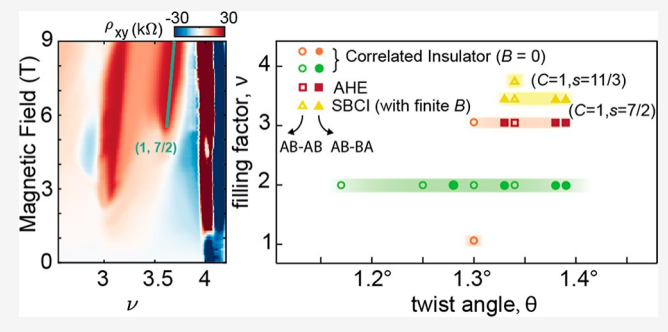
ACCESS |

III Metrics & More

Article Recommendations

Supporting Information

ABSTRACT: Twisted double bilayer graphene (tDBG) has emerged as a rich platform for studying strongly correlated and topological states, as its flat bands can be continuously tuned by both a perpendicular displacement field and a twist angle. Here, we construct a phase diagram representing the correlated and topological states as a function of these parameters, based on measurements of over a dozen tDBG devices encompassing two distinct stacking configurations. We find a hierarchy of symmetry-broken states that emerge sequentially as the twist angle approaches an apparent optimal value of $\vartheta\approx 1.34^\circ$. Nearby this angle, we discover a symmetry-broken Chern insulator (SBCI) state associated with a band filling of 7/2 as well as an incipient



SBCI state associated with 11/3 filling. We further observe an anomalous Hall effect at zero field in all samples supporting SBCI states, indicating spontaneous time-reversal symmetry breaking and possible moire unit cell enlargement at zero magnetic field.

KEYWORDS: symmetry-broken Chern insulators, twisted double bilayer graphene, anomalous Hall effect, moire

he flat bands found in the growing family of graphenebased moire materials offer a valuable platform for studying the interplay of strong correlations and topology. 1,2 Twisted double bilayer graphene (tDBG), composed of two slightly relatively rotated sheets of Bernal bilayer graphene, has been the focus of significant research attention³⁻¹⁵ owing to its exceptional tunability with perpendicular displacement field, 3-6 twist angle, and pressure. 12 Compared with twisted bilayer graphene (tBLG), in which strongly correlated states occur over a very narrow range near the magic angle of ≈1.1°, tDBG hosts correlated states over a wider range of twist angles due to its lack of a singular "magic angle" from theory. A wide variety of correlated phenomena have been reported already in tDBG, including states that are spin-polarized, 4,5 valley-polarized, 13 spin-valley-polarized, 15 and intervalley-coherent, 16 as well as a correlated electron-hole state, 8 the anomalous Hall effect (AHE),14 and superconductivity in samples interfaced with WSe₂. 17 Despite this, the phase diagram with respect to the twist angle has yet to be fully mapped, and it remains unclear whether there exist optimal twist angles for observing these phenomena.

In this work, we study more than a dozen tDBG devices to systematically construct such a phase diagram. The devices span both stacking configurations of the two inner graphene sheets, distinguished by whether the two Bernal graphene sheets are rotated slightly away from 0° (AB-AB) or 60° (AB-BA) (see as indicated in Figures 1a,b and Figure S1).

Previous studies have concentrated on the AB-AB case. Here, we find that tDBG can host symmetry-broken Chern insulator (SBCI) states, likely connected to spontaneous translational symmetry breaking of the moire unit cell. We additionally find that these states might be associated with an anomalous Hall effect at a zero magnetic field. The observation of magnetic hysteresis at fractional band filling suggests that the translational symmetry breaking may persist down to a zero field. Surprisingly, although our band structure calculations at zero field indicate that the Chern number should be different in the AB-AB and AB-BA cases (Figure 1c; see also Figure S2), we observe similar SBCI states at high field for both stacking configurations.

Our study included six AB-BA samples with ϑ varying from 1.06° to 1.39° and seven AB-AB samples with ϑ' varying from 1.17° to 1.53° (Table 1). Figures 1d and 1e show maps of the longitudinal resistivity, $\rho_{xx'}$ versus carrier density, n, and displacement field, D (see the Supporting Information for definition) for AB-AB device S1 (ϑ = 1.34°) and AB-BA device O1 (ϑ' = 1.39°), respectively. The filling factor, ν , is

Received: September 6, 2023 Revised: November 15, 2023 Accepted: November 16, 2023 Published: November 20, 2023





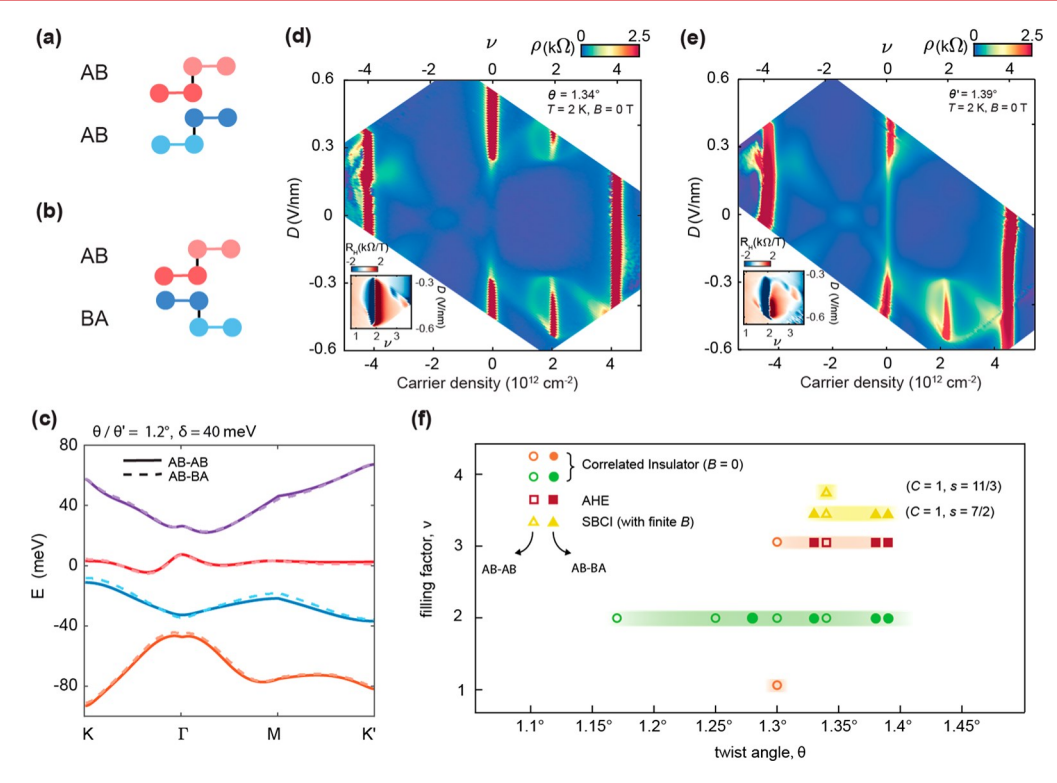


Figure 1. Hierarchy of correlated and topological phases observed in tDBG in both stacking configurations. (a, b) Side-view lattice schematics of AB-AB and AB-BA tDBG. AB-AB (AB-BA) tDBG is composed of two Bernal stacked graphene bilayers with the same (opposite) orientation. (c) Calculated band structure of $\vartheta=1.2^{\circ}$ (AB-AB, solid line) and $\vartheta'=1.2^{\circ}$ (AB-BA, dashed line) tDBG, with interlayer potential $\delta=40$ meV. The red bands denote the lowest moire conduction band. The Chern number in the AB-AB (AB-BA) stacking is C=2 (1). (d, e) Resistivity ρ_{xx} maps of $\vartheta=1.34^{\circ}$ (AB-AB) and $\vartheta'=1.39^{\circ}$ (AB-BA) devices, respectively. Measurements were taken at T=2 K and zero magnetic field. Insets shows the zoomed-in Hall coeficient R_{H} at $|\mathcal{B}|=0.5$ T, focusing on the correlated states. (f) Summary of the correlated and topological states observed in 13 tDBG devices. Correlated insulating states, states exhibiting the AHE, and SBCI states are represented by circle, square, and triangle markers, respectively. The AB-AB (AB-BA) stacking is denoted by open (closed) markers. The green and orange shading denotes the range of twist angles over which symmetry-broken metallic states are observed, identified by sign reversals in the low-field Hall effect. States denoted by (C, S) correspond to SBCIs observed in a magnetic field.

Table 1. Hierarchy of Correlated and Topological Phases in Twisted Double Bilayer Graphene; Summary of the Correlated and Topological States Observed in 13 tDBG Samples^a

twist angle	stacking configuration	v = 2	v = 3	AHEat $v = 3$	SBCI
1.06	AB-BA	none	none	/	/
1.17	AB-BA	halo only	none	/	none
1.17	AB-AB	CI with halo	none	/	/
1.25	AB-AB	CI with halo	none	/	/
1.28	AB-BA	CI with halo	none	/	none
1.30	AB-AB	CI with halo	CI with halo	no AHE	none
1.33	AB-BA	CI with halo	resistive state with halo	AHE	(1, 7/2)
1.34	AB-AB	CI with halo	halo only	/	/
1.34	AB-AB	CI with halo	halo only	AHE	(1, 7/2), (1, 11/3)
1.38 (h-BN aligned)	AB-BA	CI with halo	halo only	AHE	(1, 7/2)
1.39	AB-BA	CI with halo	halo only	AHE	(1, 7/2)
1.41	AB-AB	resistive state with halo	none	no AHE	none
1.53	AB-AB	none	none	/	/

"Samples are presented in order of ascending twist angle and labeled with their nominal stacking configuration. Absence of the correlated and topological states are labeled specifically by "none" while "/" labels lack of available measurements at the mK temperature range to properly determine. Here, "CI" denotes a correlated insulator, "halo" denotes a symmetry-broken metallic state forming a halo shape in the dual-gate map, and "AHE" denotes the anomalous Hall effect nearby filling factor v = 3. Note that AHE near fractional filling v = 3.5 is observed only in the $\vartheta' = 1.39$ ° AB-BA Sample. (C, s) labels the Chern number and band filling index of the observed symmetry-broken Chern insulators.

shown on the top axis, where $v = \pm 4$ corresponds to full filling of the lowest moire conduction and valence minibands. The data are consistent with measurements on AB-AB tDBG detailed extensively elsewhere.³⁻⁷ In brief, one sees gapped

states at v = 0 and ± 4 that are tuned by D, a cross-like resistive feature in the region v < 0 reflecting van Hove singularities in the valence band, and a "halo" feature around the insulating states at v = +2 marking the emergence of symmetry-broken

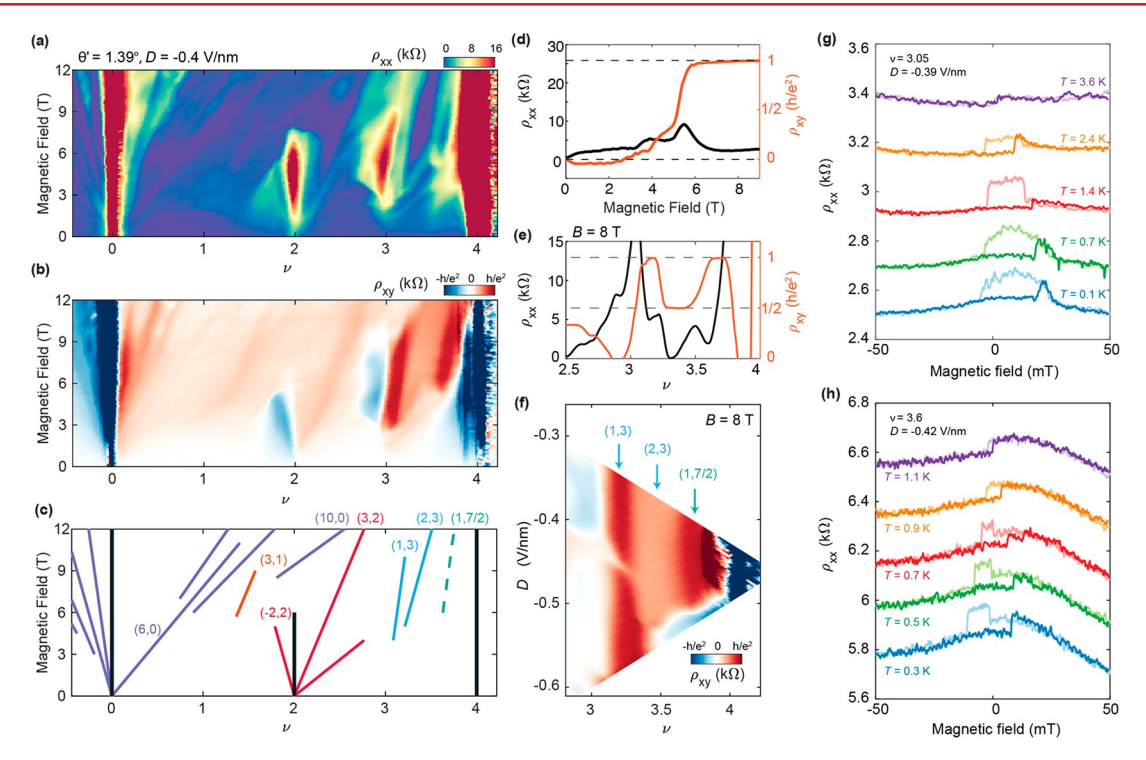


Figure 2. Symmetry-broken Chern insulator and anomalous Hall effect. (a, b) Landau fan measurements of the longitudinal ρ_{xx} and Hall resistivity ρ_{xy} at D=-0.4 V/nm in a $\vartheta'=1.39^\circ$ AB-BA sample. Data are taken at 100 mK. (c) Schematics of all observed gapped states in (a, b). Several main gapped states are labeled by their respective (C, S) values. Colors differentiate different values of S. Black vertical lines (with C=0) denote topologically trivial insulating states. The green dashed line denotes the (1, 7/2) symmetry-broken Chern insulator. (d) Line cuts of ρ_{xx} and ρ_{xy} acquired along the trajectory of the (1, 7/2) SBCI. (e) Line cuts of ρ_{xx} and ρ_{xy} acquired at fixed magnetic field, B=8 T. (d) and (e) are acquired from a different data set as shown in Figure S5. (f) ρ_{xy} map as a function of D and V, at B=8 T. Blue arrows denote Chern insulators associated with S=3, and the green arrow denotes the (1, 7/2) SBCI. ρ_{xy} maps at other B are shown in Figure S6. (g, h) ρ_{xx} measured as magnetic field is swept back and forth at (g) V=3.05, D=-0.39 V/nm, and (h) V=3.6, D=-0.42 V/nm. The data taken at different temperatures are offset vertically for clarity.

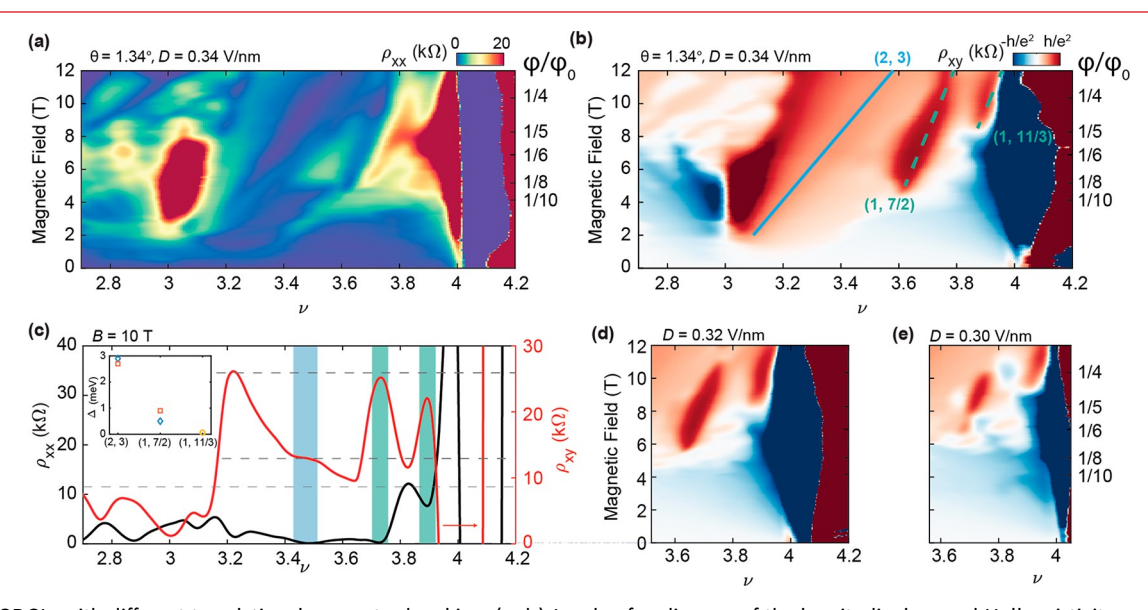


Figure 3. SBCIs with different translational symmetry breaking. (a, b) Landau fan diagram of the longitudinal ρ_{xx} and Hall resistivity ρ_{xy} at D=0.34 V/nm in a $\vartheta=1.34^\circ$ AB-AB tDBG sample. Data are taken at 100 mK. Schematics of main gapped states are overlaid in panel b, labeled by their respective (C, s) values, using the same color coding as in Figure 2. The green dashed lines denote the (1, 7/2) and the (1, 11/3) SBCIs. (c) Line cuts of ρ and ρ from panels a and b at ρ and ρ from panels a and b at ρ are emphasized by the green shadings. The nearby quantized (2, 3) Chern insulator is marked by the blue shading. The inset shows the thermal activation gap of the (2,3), (1, 7/2), and (1, 11/3) states. The blue diamonds denote data from the θ ' = 1.39° AB-BA sample at ρ = -0.4 V/nm with ρ = 8 T. The orange square denote data from the θ = 1.34° AB-AB sample at ρ = 0.4 V/nm with ρ = 9 T. (d, e) Landau fan diagram of ρ and ρ = 0.32 V/nm and ρ = 0.30 V/nm, respectively.

correlated metallic and insulating states. Measurements of the antisymmetrized Hall coeficient, $R_{\rm H}=(R_{\rm xy}[B]-R_{\rm xy}[-B])/(2B)$, further reveal incipient symmetry-broken states at v=+3. All the same features are seen in the AB–BA devices (see also Figures S3 and S4), consistent with the nearly identical calculated band dispersions of the AB–AB and AB–BA types (Figure 1c). Figure 1f summarizes the correlated and topological phases observed as a function of twist angle, which will be elaborated on below.

Our primary finding is the emergence of SBCI states in both AB-BA and AB-AB tDBG, as detailed in Figures 2 and 3, respectively. We first analyze the evidence of topological states in the AB-BA samples. Figures 2a and 2b show Landau fan diagrams of ρ_{xx} and ρ_{xy} acquired at D = -0.40 V/nm in device O1. We see signs of a variety of gapped states, each characterized by a sharp suppression of ρ_{xx} and (nearly) quantized $ho_{_{_{XV'}}}$ that evolve along linear trajectories described by the equation $v = Cn_{\varphi} + s$, where n_{φ} is the number of magnetic flux quanta per moire cell, the integer C is the Chern number, and s is the band filling index (corresponding to the number of electrons per moire unit cell). 18 Figure 2c is a schematic showing the trajectories of the more robust gapped states. States with $C \neq 0$ and s = 0, equivalent to integer quantum Hall (IQH) states, are denoted in purple. States with $C \neq 0$ and integer s, known as Chern insulators (CI), are denoted in orange (s = 1), red (s = 2), and blue (s = 3). Topologically trivial (C = 0) insulating states are denoted in black.

The IQH and CI states seen here are all consistent with gapped states predicted by the Hofstadter model $^{\rm 18-22}$ and can be understood in the context of Hofstadter sub-band ferromagnetism.²³⁻²⁸ However, we observe an additional robust gapped state with integer C = 1 but with a fractional band filling index s = 7/2 (denoted by the green dashed line in Figure 2c). Figure 2d shows that this state emerges abruptly above $B \approx 6$ T and exhibits a quantization of the Hall resistivity to $\rho_{xy} = h/e^2$ (Figure 2e; see also Figure S5). Such a gapped state, arising at a partial filling of a Hofstadter band, can only be explained by incorporating the effects of strong Coulomb interactions that go beyond simple isospin polar-associated with the formation of a SBCI, 23,29,30 in which Coulomb interactions favor the spontaneous formation of a topological charge density wave state.²⁰⁻²² Given that this gapped state emerges upon doping beyond three electrons per moire unit cell, the SBCI most likely forms within a single partially occupied moire sub-band with fully lifted isospin degeneracy. An s = 7/2 SBCI state can arise owing to a spontaneous doubling of the area of the original moire unit cell.31-33 The corresponding density wave folds the moire Brillouin zone, thereby doubling the number of moire minibands. For a state with s = 7/2, the SBCI corresponds to a complete filling of seven out of the eight available moire conduction bands. Maps of $\rho_{_{\!\mathit{XY}}}$ acquired at fixed magnetic fields (Figure 2f and Figure S6), combined with additional Landau fan diagrams taken at different values of D (Figure S7), collectively show that the SBCI state persists over an extended range of D rather than a singular value. The same C = 1, s = 7/2 SBCI state was also observed in two other AB-BA samples with $\vartheta' = 1.33^{\circ}$ and $\vartheta' = 1.38^{\circ}$ (Figure S8).

In addition to the SBCI at a high magnetic field, we also see an AHE at zero field. Figure 2g shows measurements of ρ_{xx} as the magnetic field is swept back and forth through zero at $\nu = 3.05$ and D = -0.39 V/nm at a series of temperatures T (see

also Figure S9). The hysteresis seen at low T at this filling implies that orbital magnetism is present, and hence, timereversal symmetry is broken. Despite the nominally longitudinal contact geometry, our measurements show the squareloop-type behavior expected of a Hall geometry. This is likely the result of a mosaic of magnetic domains^{34,35} in our sample resulting from structural disorder of the moire pattern. Consistent with such a disordered domain picture, the details of the hysteresis change upon thermal cycling (Figure S10a). The small amplitude of the AHE (much less than h/e^2) can also readily be explained by domains, although it is also possible that the ground state is only partially isospin polarized and not fully gapped. We also observed the AHE at $\nu = 3$ in two other AB-BA samples with $\vartheta' = 1.33^{\circ}$ and 1.38° (Figure S10). Notably, the AHE can sometimes be seen even far from v = 3, as illustrated in Figure 2h for v = 3.61 (see also Figure S11). This AHE near v = 7/2 suggests that the topological charge density wave state responsible for the SBCI at high field may still be present at zero field (see detailed discussion in the Supporting Information and Figures S12-S14). Similar observations have been reported in twisted monolayer-bilayer graphene.30

Returning to the AB-AB case (Figure 3), we find a similar SBCI with C = 1 and s = 7/2 emerging abruptly above B = 5 T, as seen in the Landau fan diagram taken at D = -0.34 V/nm in device S2 (Figure 3a,b). The trajectories of selected gapped states are overlaid on top of the ρ_{yy} Landau fan in Figure 3b, which can be compared with Figure 2c. Here, however, a second C = 1 state emerges abruptly above 9 T with a fractional band filling index s = 11/3. Analogous to the reasoning for the 7/2 state above, such a state can arise upon filling 11 of the 12 moire sub-bands in an enlarged unit cell with triple the moire unit cell area. Figure 3c shows a line cut of ρ and ρ_{xy} at B=10 T, where the 7/2 SBCI and incipient 11/3 SBCI states (indicated by green shading) are both present. Their coexistence persists over a small range of D (Figure 3d,e). Because of the small thermal activation gap of the s = 11/3 SBCI (Figure 3c inset, Figures S15 and S16), the Hall resistivity ρ_{xy} only reaches about 80% of h/e^2 at 100 mK. The s=7/2 and 11/3 states should be distinguishable based on their different electron density modulations in real space which could be observable in scanning tunneling microscopy experiments.

Notably, the s = 7/2 and 11/3 states both have a Chern number of C = 1 despite the presumed difference in their unit cell areas. Both appear to emerge out of a parent state with C =2, determined by identifying the most robust of the s = 3 states in the Landau fan diagram (Figure 3a,b). A C = 2 Chern band can be mapped onto a two-component quantum Hall system. In such a model, the s = 7/2 SBCI can be understood as a spontaneously polarized state of this two-component system? essentially, a lattice analogue of the typical quantum Hall ferromagnet. $^{31-33}$ In a band with C=2, the Berry curvature can partition evenly into each of the two components, consistent with the observed C = 1 of the SBCI when the degeneracy is lifted. However, the s = 11/3 state is more complicated in this model because a two-component C = 2state cannot be evenly partitioned into three sub-bands with integer Chern numbers. Such a state thus requires either a nonuniform partitioning of the Chern band into different subbands or a dynamical renormalization of the Chern number of the parent sub-band upon doping (i.e., from C = 2 to C = 3).

Therefore, the question of how the s=11/3 state has C=1 requires further theoretical attention.

Given that our band structure modeling suggests a different valley Chern number for the AB-AB and AB-BA configurations, it is surprising that we see little apparent dependence on the stacking type experimentally. One possibility is that our measurements are not sensitive to this difference in the valley Chern number. For example, the spin-polarized state at v = 2does not provide information to this end because occupying both valleys results in a total Chern number of zero, irrespective of the value of the valley Chern number of the band. In contrast, a spin-valley polarized state at v = 3 would have an overall Chern number equal to the valley Chern number. However, the lack of a well-quantized AHE in our samples prevents us from exploiting this fact as a means of distinguishing the valley Chern number between the two stacking configurations. In principle, the dominant Chern insulators seen at a high magnetic field can also help distinguish the valley Chern number. Exploring these differences, however, requires careful modeling of the high-field Hofstadter minibands and their associated Chern numbers, which are beyond the scope of this work. We last note that it is possible to misidentify the stacking order of a given sample in the case where a strain soliton separated the two stacked regions of bilayer graphene in the exfoliated flake,³⁶ unintentionally reversing the intended stacking order.

We conclude by returning to the summary of the correlated and topological states observed in our 13 tDBG devices, shown in Figure 1f. Overall, we see a clear pattern of states emerging within well-defined ranges of twist angle, symmetric with respect to D field orientations except for the one device additionally aligned with h-BN (see discussion on the aligned case in the Supporting Information and Figures S17-S18). The symmetry-broken state at v = 2 is the most robust, seen in devices with twist angles between 1.17° and 1.41°. An additional symmetry-broken state occurs in the vicinity of ν = 3 for twist angles between 1.30° and 1.39°, with an incipient insulating state seen in a single device⁷ with $\vartheta = 1.30^{\circ}$ (see also ref 14). Similarly, a symmetry-broken state at v = 1 emerges only at zero field in the device with $\vartheta = 1.30^{\circ}$. All devices with twist angles between 1.33° and 1.39° exhibit the AHE at B = 0and at least one SBCI at a high magnetic field. The device with $\vartheta = 1.34^{\circ}$ also exhibits an incipient s = 11/3 SBCI. Taken together, our observations suggest that the richest set of correlated and topological phases is found in tDBG samples with twist angles within the range ≈1.30°-1.39°. Therefore, although flat bands in tDBG can be formed over an extended range of twist angles owing to the tunability of the bands with displacement field, we have identified a narrow range of twist angles over which the strength of correlations appears to be greatest.

ASSOCIATED CONTENT

Data Availability Statement

All data that support the plots within this paper and other findings of this study are available from the corresponding author upon reasonable request. Source data are provided with this paper.

* Supporting Information

The Supporting Information is available free of charge at https://pubs.acs.org/doi/10.1021/acs.nanolett.3c03414.

Experimental method; band structure calculation of AB-BA tDBG; discussion on AHE near filling factor 7/ 2; theory of topological charge density wave states in tDBG; discussion on relationship between the AHE and the high field Chern insulators; SBCI state in tDBG with additional h-BN alignment; dual gate maps in additional AB-BA tDBG devices; symmetry breaking metallic states in AB-BA tDBG; additional characterization of (1, 7/2) SBCI in device O1; evolution of Chern insulators and the (1, 7/2) SBCI with magnetic field in device O1; Landau fan diagrams in device O1 at other D; robust SBCI at T = 2 K observed in additional AB-BA tDBG devices; temperature dependence of the AHE near v = 3 in device O1; AHE near v = 3 in three AB-BA tDBG devices; temperature dependence of the AHE near v = 3.5 in device O1; isolated AHE near v = 3.5 and v = 7/2 in device O1; additional filling factor vdependence and displacement field D dependence of anomalous Hall effect; temperature dependence and energy gaps of the Chern insulators in device O1; temperature dependence and energy gaps of the Chern insulators in device S2; robust SBCI with additional top hBN alignment; absence of the (1, 7/2) SBCI in ϑ = 1.30° AB-AB tDBG; absence of the AHE in $\vartheta = 1.30^{\circ}$ AB-AB tDBG (PDF)



AUTHOR INFORMATION

Corresponding Authors

Matthew Yankowitz – Department of Physics, University of Washington, Seattle, Washington 98195, United States; Department of Materials Science and Engineering, University of Washington, Seattle, Washington 98195, United States; orcid.org/0000-0002-5637-9203; Email: myank@uw.edu

Xiaodong Xu – Department of Physics, University of Washington, Seattle, Washington 98195, United States; Department of Materials Science and Engineering, University of Washington, Seattle, Washington 98195, United States; orcid.org/0000-0003-0348-2095; Email: xuxd@uw.edu

Authors

Minhao He – Department of Physics, University of Washington, Seattle, Washington 98195, United States; orcid.org/0000-0002-4769-0438

Jiaqi Cai – Department of Physics, University of Washington, Seattle, Washington 98195, United States; orcid.org/ 0000-0002-7829-9554

Ya-Hui Zhang – Department of Physics and Astronomy, Johns Hopkins University, Baltimore, Maryland 21218, United States

Yang Liu – Department of Physics, University of Washington, Seattle, Washington 98195, United States

Yuhao Li – Department of Physics, University of Washington, Seattle, Washington 98195, United States; Ocid.org/ 0000-0003-4469-5468

Takashi Taniguchi – International Center for Materials Nanoarchitectonics, National Institute for Materials Science, Tsukuba 305-0044, Japan; ⊙ orcid.org/0000-0002-1467-3105

Kenji Watanabe – Research Center for Functional Materials, National Institute for Materials Science, Tsukuba 305-0044, Japan; ⊙ orcid.org/0000-0003-3701-8119 David H. Cobden - Department of Physics, University of Washington, Seattle, Washington 98195, United States

Complete contact information is available at: https://pubs.acs.org/10.1021/acs.nanolett.3c03414

Author Contributions

M.H. and J.C. contributed equally to this work. X.X. and M.Y. conceived and supervised the experiment. M.H. and J.C. fabricated the devices and performed the measurements. Y.Z. performed the calculations. Y.Liu and Y.Li contributed to fabrication of AB-AB stacked devices. D.H.C. assisted with measurements in the dilution refrigerator. K.W. and T.T. provided the bulk hBN crystals. M.H., J.C., M.Y., and X.X. analyzed the data and wrote the paper with input from all authors.

Notes

The authors declare no competing financial interest.

|?

ACKNOWLEDGMENTS

This research was primarily supported by the U.S. National Science Foundation through the UW Molecular Engineering Materials Center (MEM-C), a Materials Research Science and Engineering Center (DMR-1719797 and DMR-2308979), including the use of facilities and instrumentation provide by the MEM-C Shared Facilities. M.H. and M.Y. acknowledge support from the Army Research Ofice under Grant W911NF-20-1-0211. Y.H.Z. was supported by the National Science Foundation under Grant DMR-2237031. X.X. and M.Y. acknowledge support from the State of Washington funded Clean Energy Institute. This work made use of a dilution refrigerator system which was provided by NSF DMR1725221. K.W. and T.T. acknowledge support from the Elemental Strategy Initiative conducted by the MEXT, Japan, Grant JPMXP0112101001, JSPS KAKENHI Grant JP20H00354 and the CREST (JPMJCR15F3), JST.

REFERENCES

- (1) Balents, L.; Dean, C. R.; Efetov, D. K.; Young, A. F. Superconductivity and Strong Correlations in Moire Flat Bands. *Nat. Phys.* 2020, *16* (7), 725–733.
- (2) Andrei, E. Y.; Efetov, D. K.; Jarillo-Herrero, P.; MacDonald, A. H.; Mak, K. F.; Senthil, T.; Tutuc, E.; Yazdani, A.; Young, A. F. The Marvels of Moire Materials. *Nat. Rev. Mater.* 2021, *6* (3), 201–206.
- (3) Burg, G. W.; Zhu, J.; Taniguchi, T.; Watanabe, K.; MacDonald, A. H.; Tutuc, E. Correlated Insulating States in Twisted Double Bilayer Graphene. *Phys. Rev. Lett.* 2019, *123* (19), 197702.
- (4) Cao, Y.; Rodan-Legrain, D.; Rubies-Bigorda, O.; Park, J. M.; Watanabe, K.; Taniguchi, T.; Jarillo-Herrero, P. Tunable Correlated States and Spin-Polarized Phases in Twisted Bilayer-Bilayer Graphene. *Nature* 2020, *583* (7815), 215–220.
- (5) Liu, X.; Hao, Z.; Khalaf, E.; Lee, J. Y.; Ronen, Y.; Yoo, H.; Najafabadi, D. H.; Watanabe, K.; Taniguchi, T.; Vishwanath, A.; Kim, P. Tunable Spin-Polarized Correlated States in Twisted Double Bilayer Graphene. *Nature* 2020, *583* (7815), 221–225.
- (6) Shen, C.; Chu, Y.; Wu, Q.; Li, N.; Wang, S.; Zhao, Y.; Tang, J.; Liu, J.; Tian, J.; Watanabe, K.; Taniguchi, T.; Yang, R.; Meng, Z. Y.; Shi, D.; Yazyev, O. V.; Zhang, G. Correlated States in Twisted Double Bilayer Graphene. *Nat. Phys.* 2020, *16* (5), 520–525.
- (7) He, M.; Li, Y.; Cai, J.; Liu, Y.; Watanabe, K.; Taniguchi, T.; Xu, X.; Yankowitz, M. Symmetry Breaking in Twisted Double Bilayer Graphene. *Nat. Phys.* 2021, *17* (1), 26–30.
- (8) Rickhaus, P.; de Vries, F. K.; Zhu, J.; Portoles, E.; Zheng, G.; Masseroni, M.; Kurzmann, A.; Taniguchi, T.; Watanabe, K.; MacDonald, A. H.; Ihn, T.; Ensslin, K. Correlated Electron-Hole

- State in Twisted Double-Bilayer Graphene. *Science* 2021, *373* (6560), 1257–1260.
- (9) Liu, X.; Chiu, C.-L.; Lee, J. Y.; Farahi, G.; Watanabe, K.; Taniguchi, T.; Vishwanath, A.; Yazdani, A. Spectroscopy of a Tunable Moire System with a Correlated and Topological Flat Band. *Nat. Commun.* 2021, *12* (1), 2732.
- (10) Zhang, C.; Zhu, T.; Kahn, S.; Li, S.; Yang, B.; Herbig, C.; Wu, X.; Li, H.; Watanabe, K.; Taniguchi, T.; Cabrini, S.; Zettl, A.; Zaletel, M. P.; Wang, F.; Crommie, M. F. Visualizing Delocalized Correlated Electronic States in Twisted Double Bilayer Graphene. *Nat. Commun.* 2021, *12* (1), 2516.
- (11) Wang, Y.; Herzog-Arbeitman, J.; Burg, G. W.; Zhu, J.; Watanabe, K.; Taniguchi, T.; MacDonald, A. H.; Bernevig, B. A.; Tutuc, E. Bulk and Edge Properties of Twisted Double Bilayer Graphene. *Nat. Phys.* 2022, *18*, 48–53.
- (12) Szentpeteri, B.; Rickhaus, P.; de Vries, F. K.; Marffy, A.; Fulop, B.; Tovari, E.; Watanabe, K.; Taniguchi, T.; Kormanyos, A.; Csonka, S.; Makk, P. Tailoring the Band Structure of Twisted Double Bilayer Graphene with Pressure. *Nano Lett.* 2021, *21*, 8777.
- (13) Liu, L.; Zhang, S.; Chu, Y.; Shen, C.; Huang, Y.; Yuan, Y.; Tian, J.; Tang, J.; Ji, Y.; Yang, R.; Watanabe, K.; Taniguchi, T.; Shi, D.; Liu, J.; Yang, W.; Zhang, G. Isospin Competitions and Valley Polarized Correlated Insulators in Twisted Double Bilayer Graphene. *Nat. Commun.* 2022, *13* (1), 3292.
- (14) Kuiri, M.; Coleman, C.; Gao, Z.; Vishnuradhan, A.; Watanabe, K.; Taniguchi, T.; Zhu, J.; MacDonald, A. H.; Folk, J. Spontaneous Time-Reversal Symmetry Breaking in Twisted Double Bilayer Graphene. *Nat. Commun.* 2022, *13* (1), 6468.
- (15) Liu, L.; Lu, X.; Chu, Y.; Yang, G.; Yuan, Y.; Wu, F.; Ji, Y.; Tian, J.; Watanabe, K.; Taniguchi, T.; Du, L.; Shi, D.; Liu, J.; Shen, J.; Lu, L.; Yang, W.; Zhang, G. Observation of First-Order Quantum Phase Transitions and Ferromagnetism in Twisted Double Bilayer Graphene. *Phys. Rev. X* 2023, *13* (3), 031015.
- (16) He, M.; Zhang, Y.-H.; Li, Y.; Fei, Z.; Watanabe, K.; Taniguchi, T.; Xu, X.; Yankowitz, M. Competing Correlated States and Abundant Orbital Magnetism in Twisted Monolayer-Bilayer Graphene. *Nat. Commun.* 2021, *12* (1), 4727.
- (17) Su, R.; Kuiri, M.; Watanabe, K.; Taniguchi, T.; Folk, J. Superconductivity in Twisted Double Bilayer Graphene Stabilized by WSe2. *Nat. Mater.* 2023, *22*, 1332.
- (18) Wannier, G. H. A Result Not Dependent on Rationality for Bloch Electrons in a Magnetic Field. *Phys. Stat. Sol.* (b) 1978, 88 (2), 757–765.
- (19) Hofstadter, D. R. Energy Levels and Wave Functions of Bloch Electrons in Rational and Irrational Magnetic Fields. *Phys. Rev. B* 1976, *14* (6), 2239–2249.
- (20) Dean, C. R.; Wang, L.; Maher, P.; Forsythe, C.; Ghahari, F.; Gao, Y.; Katoch, J.; Ishigami, M.; Moon, P.; Koshino, M.; Taniguchi, T.; Watanabe, K.; Shepard, K. L.; Hone, J.; Kim, P. Hofstadter's Butterfly and the Fractal Quantum Hall Effect in Moire Superlattices. *Nature* 2013, *497* (7451), 598–602.
- (21) Hunt, B.; Sanchez-Yamagishi, J. D.; Young, A. F.; Yankowitz, M.; LeRoy, B. J.; Watanabe, K.; Taniguchi, T.; Moon, P.; Koshino, M.; Jarillo-Herrero, P.; Ashoori, R. C. Massive Dirac Fermions and Hofstadter Butterfly in a van Der Waals Heterostructure. *Science* 2013, *340* (6139), 1427–1430.
- (22) Ponomarenko, L. A.; Gorbachev, R. V.; Yu, G. L.; Elias, D. C.; Jalil, R.; Patel, A. A.; Mishchenko, A.; Mayorov, A. S.; Woods, C. R.; Wallbank, J. R.; Mucha-Kruczynski, M.; Piot, B. A.; Potemski, M.; Grigorieva, I. V.; Novoselov, K. S.; Guinea, F.; Fal'ko, V. I.; Geim, A. K. Cloning of Dirac Fermions in Graphene Superlattices. *Nature* 2013, 497 (7451), 594–597.
- (23) Saito, Y.; Ge, J.; Rademaker, L.; Watanabe, K.; Taniguchi, T.; Abanin, D. A.; Young, A. F. Hofstadter Subband Ferromagnetism and Symmetry-Broken Chern Insulators in Twisted Bilayer Graphene. *Nat. Phys.* 2021, *17* (4), 478–481.
- (24) Wu, S.; Zhang, Z.; Watanabe, K.; Taniguchi, T.; Andrei, E. Y. Chern Insulators, van Hove Singularities and Topological Flat Bands

- in Magic-Angle Twisted Bilayer Graphene. *Nat. Mater.* 2021, 20 (4), 488–494.
- (25) Nuckolls, K. P.; Oh, M.; Wong, D.; Lian, B.; Watanabe, K.; Taniguchi, T.; Bernevig, B. A.; Yazdani, A. Strongly Correlated Chern Insulators in Magic-Angle Twisted Bilayer Graphene. *Nature* 2020, 588 (7839), 610–615.
- (26) Das, I.; Lu, X.; Herzog-Arbeitman, J.; Song, Z.-D.; Watanabe, K.; Taniguchi, T.; Bernevig, B. A.; Efetov, D. K. Symmetry-Broken Chern Insulators and Rashba-like Landau-Level Crossings in Magic-Angle Bilayer Graphene. *Nat. Phys.* 2021, *17*, 710.
- (27) Choi, Y.; Kim, H.; Peng, Y.; Thomson, A.; Lewandowski, C.; Polski, R.; Zhang, Y.; Arora, H. S.; Watanabe, K.; Taniguchi, T.; Alicea, J.; Nadj-Perge, S. Correlation-Driven Topological Phases in Magic-Angle Twisted Bilayer Graphene. *Nature* 2021, *589* (7843), 536–541.
- (28) Park, J. M.; Cao, Y.; Watanabe, K.; Taniguchi, T.; Jarillo-Herrero, P. Flavour Hund's Coupling, Chern Gaps and Charge Diffusivity in Moire Graphene. *Nature* 2021, *592* (7852), 43–48.
- (29) Spanton, E. M.; Zibrov, A. A.; Zhou, H.; Taniguchi, T.; Watanabe, K.; Zaletel, M. P.; Young, A. F. Observation of Fractional Chern Insulators in a van Der Waals Heterostructure. *Science* 2018, *360*, No. 62.
- (30) Polshyn, H.; Zhang, Y.; Kumar, M. A.; Soejima, T.; Ledwith, P.; Watanabe, K.; Taniguchi, T.; Vishwanath, A.; Zaletel, M. P.; Young, A. F. Topological Charge Density Waves at Half-Integer Filling of a Moire Superlattice. *Nat. Phys.* 2022, *18*, 42.
- (31) Barkeshli, M.; Qi, X.-L. Topological Nematic States and Non-Abelian Lattice Dislocations. *Phys. Rev. X* 2012, *2* (3), 031013.
- (32) Wu, Y.-L.; Regnault, N.; Bernevig, B. A. Bloch Model Wave Functions and Pseudopotentials for All Fractional Chern Insulators. *Phys. Rev. Lett.* 2013, *110* (10), 106802.
- (33) Kumar, A.; Roy, R.; Sondhi, S. L. Generalizing Quantum Hall Ferromagnetism to Fractional Chern Bands. *Phys. Rev. B* 2014, *90* (24), 245106.
- (34) Tschirhart, C. L.; Serlin, M.; Polshyn, H.; Shragai, A.; Xia, Z.; Zhu, J.; Zhang, Y.; Watanabe, K.; Taniguchi, T.; Huber, M. E.; Young, A. F. Imaging Orbital Ferromagnetism in a Moire Chern Insulator. *Science* 2021, *372* (6548), 1323–1327.
- (35) Grover, S.; Bocarsly, M.; Uri, A.; Stepanov, P.; Di Battista, G.; Roy, I.; Xiao, J.; Meltzer, A. Y.; Myasoedov, Y.; Pareek, K.; Watanabe, K.; Taniguchi, T.; Yan, B.; Stern, A.; Berg, E.; Efetov, D. K.; Zeldov, E. Chern Mosaic and Berry-Curvature Magnetism in Magic-Angle Graphene. *Nat. Phys.* 2022, *18* (8), 885–892.
- (36) Ju, L.; Shi, Z.; Nair, N.; Lv, Y.; Jin, C.; Velasco, J.; Ojeda-Aristizabal, C.; Bechtel, H. A.; Martin, M. C.; Zettl, A.; Analytis, J.; Wang, F. Topological Valley Transport at Bilayer Graphene Domain Walls. *Nature* 2015, *520* (7549), 650–655.